# Atomistic deformation modes and intrinsic brittleness of $Al_4SiC_4$: A first-principles investigation

Ting Liao,[1,2] Jingyang Wang,[1,3] and Yanchun Zhou[1]
[1]*Shenyang National Laboratory for Materials Science, Institute of Metal Research, Chinese Academy of Sciences, Shenyang 110016, China*
[2]*Graduate School of Chinese Academy of Sciences, Beijing 100039, China*
[3]*International Centre for Materials Physics, Institute of Metal Research, Chinese Academy of Sciences, Shenyang 110016, China*
(Received 31 July 2006; revised manuscript received 10 October 2006; published 16 November 2006)

From crystallographic point of view, $Al_4SiC_4$ can be described as $Al_4C_3$-type and hexagonal SiC-type structural units alternatively stacked along [0001] direction. However, relationship between this layered crystal structure and mechanical properties is not fully established for $Al_4SiC_4$, except for the reported bulk modulus locating between those of $Al_4C_3$ and SiC. Based on the first-principles pseudopotential total energy method, we calculated the elastic stiffness of $Al_4SiC_4$, and reported on its ideal tensile and shear stress-strain relationships considering different structural deformation modes. Elastic properties of $Al_4SiC_4$ are dominated by the $Al_4C_3$-type structural units and exhibit similar results with those of $Al_4C_3$. Furthermore, the atomistic deformation modes of $Al_4SiC_4$ upon tensile and shear deformations are illustrated and compared with $Al_4C_3$ as well. Since the tension-induced bond breaking occurs inside the constitutive $Al_4C_3$-type unit, the ternary carbide has similar ideal tensile strength with $Al_4C_3$. On the other hand, despite the softening of strong coupling between $Al_4C_3$- and SiC-type structural units is involved in shear, the shear strength for $Al_4SiC_4$ is, however, lower than the tensile strength, since *p*-state involved Al-C bonds respond more readily to the shear deformation than to tension. In addition, based on the comparison of strain energies at the maximum stresses, i.e., ideal strengths, for both tension and shear, we suggest that structural failure occurs in tensile deformation firstly and, thus confirms an intrinsic brittleness of $Al_4SiC_4$. For crystal structure arranged in alternatively stacking configuration, such as $Al_4SiC_4$, mechanical properties can be traced back to the constituent units, and are also related to the coupling strengths between each constituent unit. The results might provide a computational method to predict ductile or brittle response of a solid to applied deformations.

DOI: 10.1103/PhysRevB.74.174112 PACS number(s): 81.05.Je, 62.20.−x, 71.20.−b

## I. INTRODUCTION

A large number of aluminum-containing ternary ceramics are among the most promising candidates for high temperature structural application and part of them as oxidation-protective multicomposition coatings.[1] Well-documented layered ternary aluminum carbides, such as $Ti_3AlC_2$, $Ti_2AlC$, and $Nb_2AlC$, have been reported to be hexagonal crystals and have many astonishing properties, such as room temperature ductility, oxidation resistance, and good damage tolerance,[2] differing dramatically from their binary counterparts. Another group of ternary aluminum carbides in the Zr-Al-C and Hf-Al-C systems were also studied. Among them $Zr_3Al_3C_5$ and $Hf_3Al_3C_5$ were determined to have the hexagonal symmetry too.[3] By means of *ab initio* pseudopotential total energy calculations,[4] $Zr_3Al_3C_5$ was predicted to have similar mechanical properties to the hard binary carbide, ZrC. As a thumb rule, many properties, particularly mechanical properties, could be traced back to the crystal structures.

These layered ternary carbides can be described as various structural units arranged alternatively along the *c* direction with different coupling strengths. For example, crystal structure of $Ti_2AlC$ or $Nb_2AlC$ is described as $Ti_2C$ or $Nb_2C$ slabs in a NaCl-type structure being intercalated and mirrored by close-packed Al atomic planes, and $Zr_3Al_3C_5$ may be viewed as the nonstoichiometric $ZrC_x$ slabs in NaCl-type structure being coupled to $Al_4C_3$-type Al-C layers.[5] The mechanical properties of these aluminum-containing ternary carbides are, therefore, determined by the coupling strengths between each structural unit, or the structural unit itself. According to previous theoretical investigations, the machinability, damage tolerance, and microscale ductility of ternary $Ti_2AlC$ and $Nb_2AlC$ phases are totally traceable to the weak coupling between the transition metal carbide units and the planar aluminum atomic layers, while the high bulk modulus and Young's moduli are originated from the strong $Ti_2C$ or $Nb_2C$ slabs.[6–8] Similarly, bonding strength analysis suggest that the strong coupling of Zr-C blocks to Al-C layers are decisive to the mechanical properties of $Zr_3Al_3C_5$.[4]

Aluminum silicon carbide, $Al_4SiC_4$, is another aluminum-containing ternary carbide and has been characterized by low theoretical density, high melting point, high heat conductivity, and excellent oxidation resistance.[9,10] If fine particles $Al_4SiC_4$ is dispersed in C/C composites, mullite $(3Al_2O_3 \cdot 2SiO_2)$ is expected to be formed directly by their oxidation and hence, an improvement of oxidation resistance is achieved for the C/C composites.[11] As illustrated in Fig. 1, $Al_4SiC_4$ may be viewed as an intergrown structure consisting of two kinds of layers. One is the Al-C slab in an $Al_4C_3$-type structure and the other consists of Si and C atoms in an arrangement similar to that in any polytype of silicon carbide, SiC. The $Al_4SiC_4$ has been widely studied and proved to be excellent in oxidation resistance at high temperature.[11,12] The bulk modulus was recently reported to be 182 GPa, which locates between those of $Al_4C_3$ and SiC.[13] For a structural ceramic with potential high-temperature applications, the correlation between the elec-

 

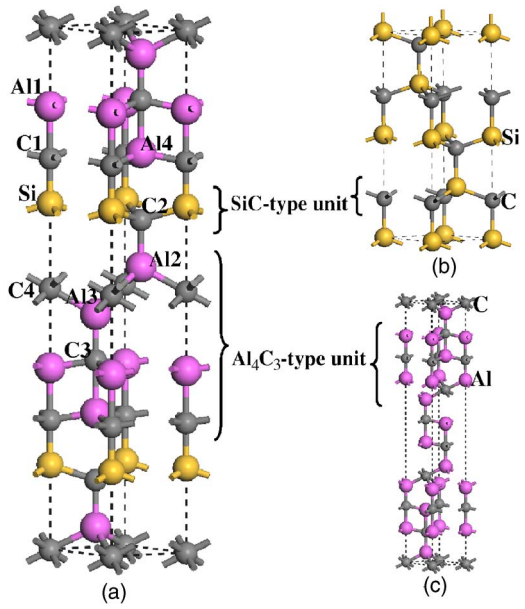


FIG. 1. (Color online) Crystal structures of (a) $Al_4SiC_4$, (b) 4H-SiC, and (c) $Al_4C_3$. The yellow, purple, and gray balls represent Al, Si, and C atoms, respectively. The Al and C atoms in $Al_4SiC_4$ are indexed with numbers according to various coordination environments.

tronic structure, crystal structure, and mechanical properties should be fully established for $Al_4SiC_4$ at first. Analogous to the above mentioned aluminum-containing ternary carbides, it is helpful to clarify how the mechanical properties of $Al_4SiC_4$ are determined by its intergrown structure or coupling strength between different structural units. Moreover, it is meaningful to generalize current analytic characteristics to further prediction of mechanical properties for other crystals stacked in layered arrangement. In this study, we computed the elastic stiffness, ideal strengths, atomistic deformation modes, and chemical bonding characteristics of $Al_4SiC_4$ using the first-principles computational scheme. The investigation aims to study possible deformation modes, and further, to show the relationship between the crystal structure and the mechanical properties. The quest for the strain energy comparison at the maximum stresses, i.e., ideal strengths, between shear and tension is also performed to unveil the intrinsic brittleness of $Al_4SiC_4$.

Predicting mechanical properties based on first-principles calculation has been frequently focused in the past decades.[14–17] First-principles study on the stress-strain relation can establish the detailed atomistic bond softening and breaking modes of materials and, thus predict the mechanical responses to applied strains. The calculated elastic constants determine the behavior of material under small deformation when the stress-strain relation is still linear. Another important parameter, which describes the behavior of material near the limit of structural stability, is the ideal strengths. The ideal tensile and shear strengths represent the upper bound stresses necessary for cleavage, slip, or fracture of the crystal. As an inherent property of crystal lattice, the strengths offer insight into the correlation between the intrinsic chemical bonding and mechanical properties.[18] Studies of the stress-strain relations and the underlying atomistic deformation processes can provide important insights into the fundamental aspects of deformation and failure modes, which are critical to understanding the mechanical properties. Moreover, ductility of a solid is controlled by the energy needed to break bonds by shear compared to that by tension.[19–21] It has been characterized that $Ti_2AlC$ and $Ti_2AlN$ yield a large ratio of tensile strength to the shear one,[22] suggesting an intrinsic ductility. The atomistic deformation modes of TiC and TiN suggest intrinsic brittleness quantitatively represented by comparable tensile to shear ideal strengths. In the present work, we hope to establish an atomistic description of the deformation modes of $Al_4SiC_4$ to further understand the correlation between structure and its properties.

The remainder of this paper is organized as follows. The computational details are described in Sec. II. In Sec. III, we present results for equilibrium geometry and elastic stiffness of $Al_4SiC_4$, together with the full set of elastic coefficients of $Al_4C_3$ and 4H-SiC for comparison. The ideal stress-strain relationship, ideal tensile, and shear strength, along with the description of atomistic deformation modes for material strained from elasticity to structural instability, are illustrated in Sec. IV. Finally, the concluding remarks are given in Sec. V.

## II. COMPUTATIONAL DETAILS

The equilibrium crystal parameters and ground-state electronic structure were calculated using the CASTEP (Ref. 23) code, in which the plane-wave pseudopotential total energy calculation was performed. Interactions of electrons with ion cores were represented by the Vanderbilt-type ultrasoft pseudopotential for Al, Si, and C atoms.[24] The electronic exchange-correlation energy was treated under the generalized gradient approximation (GGA-PW91).[25] The plane-wave basis set cutoff was set as 450 eV for all cases, which was sufficient in leading to good convergence for total energy and forces acting on the atoms. The special points sampling integration over the Brillouin zone was employed by using the Monkhorst-Pack method with $10\times10\times2$ special $k$-point meshes.[26] The tolerances for the geometry optimization were selected as the difference in total energy within $5.0\times10^{-6}$ eV/atom, the maximum ionic Hellmann-Feynman force within 0.01 eV/Å, the maximum ionic displacement within $5.0\times10^{-4}$ Å, and the maximum stress within 0.02 GPa. Increasing the plane-wave cutoff energy to 700 eV and the $k$-point meshes to $14\times14\times2$ changed the total energy and lattice constants by less than 0.003 eV/atom and 0.004%, respectively. Therefore, the present computations were precise enough to represent the ground state properties of studied compounds. To investigate the bonding strengths of different bonds, the lattice configurations were optimized at various isotropic hydrostatic pressures ranging from 0 to 50 GPa. Lattice parameters, including lattice constants and internal atomic coordinates, were modified independently to minimize the free enthalpy, interatomic forces and unit-cell stresses. The Brodyden-Fletcher-Goldfarb-Shanno (BFGS) minimization scheme[27] was used in geometry optimization.

The elastic coefficients were determined from a first-principles calculation by applying a set of given homogeneous deformations with a finite value and calculating the resulting stress with respect to optimizing the internal degrees of freedom, as implemented by Milman *et al.*[28] The criteria for convergence in optimizing atomic internal freedoms were selected as follows: difference on total energy within $1\times10^{-6}$ eV/atom, ionic Hellmann-Feynman forces within 0.002 eV/Å and maximum ionic displacement within $1\times10^{-4}$ Å. Two strain patterns, one with nonzero $\varepsilon_{11}$ and $\varepsilon_{23}$ components and other with a nonzero $\varepsilon_{33}$, generated stresses related to all five independent elastic coefficients for a unit cell with hexagonal symmetry. Three positive and three negative amplitudes were applied for each strain pattern with a maximum strain value of 0.5%. We determined the elastic coefficients from linear fits of calculated stresses as a function of strains. The compliance tensor $S$ was calculated as the inverse of the stiffness tensor, $S=C^{-1}$. Other mechanical parameters, such as bulk modulus, Young's moduli, and Poisson's ratio were calculated from the compliance tensor. The shear modulus was calculated according to the Voigt approximation.[29]

Investigation of the atomistic deformation modes was performed by straining material far beyond the elastic region. We applied a series of incremental strains to the unit cell under constant-strain-constraint condition, along the [0001](0001), $[1\bar{2}10](0001)$, and $[\bar{1}010](0001)$ strain paths, respectively, and calculated the achieved tensile and shear stresses. To ensure that the unit cell was under a uniaxial stress condition, we relaxed all other degrees of freedom (including cell constants and internal atomic coordinates) until the calculated Hellmann-Feynman stresses are less than 0.2 GPa, with constraining the applied strain. The first maximum in stress-strain curve is regarded as the ideal strength.

## III. EQUILIBRIUM GEOMETRY AND ELASTIC STIFFNESS

The equilibrium crystal structure of $Al_4SiC_4$ belongs to the $P6_3mc$ space group and is proposed as being similar to that of aluminum carbontride $Al_5C_3N$. The crystal structure of $Al_4SiC_4$ is illustrated in Fig. 1 and, the Al and C atoms are indexed with various numbers according to different coordination environments. Silicon atoms are located at 2*a* Wyckoff positions. Aluminum and carbon atoms both occupy four structurally nonequivalent positions: Al atoms have three in 2*b* and one in 2*a* Wyckoff positions, and C atoms have two in 2*a* and two in 2*b* positions, respectively. For comparison, the crystal structures of $Al_4C_3$ and 4H-SiC are also plotted. The hexagonal 4H-SiC has the smallest unit cell that contains inequivalent atomic sites with either cubic (*k*) or hexagonal (*h*) character in the complex SiC polytypes. As can be seen from Fig. 1, the structural relationships between $Al_4SiC_4$, $Al_4C_3$, and hexagonal polytype 4H-SiC are well stated. The crystal structure of $Al_4SiC_4$ can be described as an intergrown structure consisting of two kinds of layers stacking alternately along the [0001] direction. One is composed of Al and C atoms in an arrangement resembling the binary aluminum carbide, $Al_4C_3$, and the other is corner-sharing $SiC_4$ tetrahedra derived from any polytype of SiC crystal structures. Coupling between the $Al_4C_3$- and SiC-type structural units may also play a key role for the mechanical properties and structural stability of $Al_4SiC_4$. Theoretical lattice parameters of $Al_4SiC_4$, $Al_4C_3$, and 4H-SiC are listed in Table I, together with the experimental values for comparison.[13,30,31] The computed lattice constants *a* and *c* of studied compounds are in consistency with experimental data within 2% deviation. Therefore, the present first-principles computation is reliable to reproduce the equilibrium crystal structures of the compounds.

TABLE I. Theoretical and experimental lattice parameters (in Å) and $c/a$ ratio of $Al_4SiC_4$, $Al_4C_3$, and 4H-SiC.

| | Method | *a* | *c* | *c*/*a* |
|---|---|---|---|---|
| $Al_4SiC_4$ | Calc. | 3.222 | 21.352 | 6.627 |
| | Expt.[a] | 3.277 | 21.74 | 6.634 |
| $Al_4C_3$ | Calc. | 3.281 | 24.547 | 7.482 |
| | Expt.[b] | 3.331 | 24.99 | 7.502 |
| 4H-SiC | Calc. | 3.036 | 9.936 | 3.273 |
| | Expt.[c] | 3.081 | 10.085 | 3.273 |

[a]Reference 13.
[b]Reference 30.
[c]Reference 31.

To illustrate the bonding strengths in $Al_4SiC_4$, we present the bond-length contractions under various hydrostatic pressures in Fig. 2, together with the axial ratio, $c/a$, as a function of external pressure plotted in the inset. As shown in Fig. 2, the highest lying curve associates with the Si-C1 bond and shows the most resistive character to applied pressure among the illustrated bonds. The Si-C1 bond corresponds to the coupling between the $Al_4C_3$- and SiC-type structural units, which implies that an enhanced mechanical property might be achieved for $Al_4SiC_4$ compared with that of $Al_4C_3$. The lowest lying curve shows the most compressible feature and corresponds to Al1-C1 bond along the *c* direction. Since the Al1-C1 bonds locate in the $Al_4C_3$-type structural unit, $Al_4SiC_4$ is expected to be in more resemblance in mechanical properties with the binary carbide, $Al_4C_3$, because of the

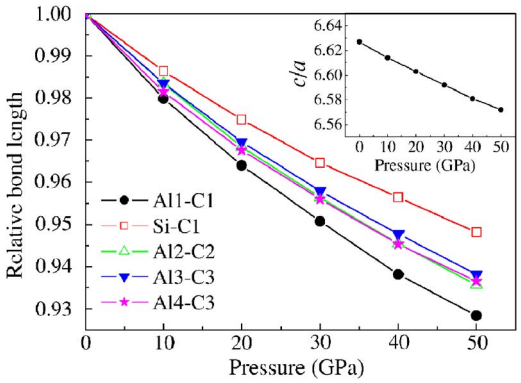


FIG. 2. (Color online) Bond-length contractions in $Al_4SiC_4$ under various pressures, together with the axial ratio $c/a$ as a function of pressure shown in the inset.

TABLE II. Calculated second order elastic constants $c_{ij}$ (in GPa) for $Al_4SiC_4$, $Al_4C_3$, and 4H-SiC.

| Compound | $c_{11}$ | $c_{12}$ | $c_{13}$ | $c_{33}$ | $c_{44}$ | $c_{66}$ |
|---|---|---|---|---|---|---|
| $Al_4SiC_4$ | 386 | 118 | 50 | 409 | 122 | 134 |
| $Al_4C_3$ | 352 | 115 | 52 | 391 | 116 | 119 |
| 4H-SiC | 532 | 102 | 48 | 577 | 175 | 215 |

weakest bonding. The other three curves, associated with Al2-C2, Al3-C3, and Al4-C3 bonds, are closed to one another, indicating similar bonding strengths against compression. The slight deviation may be due to different coordination environment of carbon atoms. With respect to the Al-C and Si-C bonds orienting along the basal plane, it is noticed that the contraction tendencies resemble those of Al2-C2, Al3-C3, and Al4-C3 bonds. The curves deviate the data of Al2-C2, Al3-C3, and Al4-C3 bonds in small magnitude. It is hard to distinguish these curves in the studied pressure range. This result shows similar bonding strength of the investigated bonds. For briefness, the bond-length contractions of bonds orienting along the basal plane are not plotted in Fig. 2.

As shown in the inset of Fig. 2, the $c/a$ ratio decreases continuously as the pressure increases up to 50 GPa. The tendency demonstrates that $c$ axis contracts more than $a$ axis does in the pressure range examined. This indicates that $Al_4SiC_4$ is stiffer in the basal plane than that parallel to the [0001] direction. Therefore, $Al_4SiC_4$ is anisotropic in elastic stiffness through the investigated pressures. Under each applied hydrostatic pressure, we optimized the crystal structure by relaxing the cell degrees of freedom with no constraint. Based on the monotonous behavior of those bond length contraction curves, no pressure-induced phase transition occurs in $Al_4SiC_4$. Strong covalent bonding between Al-C and Si-C bonds in hexagonal lattice provide no phase transition.

Table II includes computed second-order elastic constants of $Al_4SiC_4$, $Al_4C_3$, and 4H-SiC. We note that the elastic constants of $Al_4SiC_4$ are more close to those of $Al_4C_3$, but differ significantly from the corresponding values of 4H-SiC. The elastic constants $c_{11}$ and $c_{33}$, which represent stiffness against principal strains, exhibit slightly higher values for $Al_4SiC_4$ compared with those of $Al_4C_3$. The enhancements are attributed to the positive contribution of strong coupling between the $Al_4C_3$- and SiC-type structural units in $Al_4SiC_4$. The $c_{44}$ and $c_{66}$, which are related to the shear resistance in the {100} ⟨110⟩ and {010} ⟨001⟩ directions, respectively, show higher values for $Al_4SiC_4$ with respect to those of $Al_4C_3$ as well. Mechanical parameters of polycrystalline, such as bulk modulus $B$ and shear modulus $G$, are computed from the elastic coefficient tensor, and are listed in Table III. The computed bulk modulus $B$ for $Al_4SiC_4$ is 179 GPa, and is in good agreement with the experimental data, 182 GPa, obtaind by fitting the Birch-Murnaghan equation of state.[13] Compared to those of $Al_4C_3$, the bulk modulus $B$ and shear modulus $G$ of $Al_4SiC_4$ are enhanced by 9 and 11 GPa, respectively. Based on a close, but slightly higher, mechanical parameters of $Al_4SiC_4$ and $Al_4C_3$, the $Al_4C_3$-type structural units dominate the mechanical properties of $Al_4SiC_4$, while, the other constituent unit in SiC-type arrangement and the strong coupling between each structural unit also play a role in enhancing the mechanical properties of $Al_4SiC_4$.

TABLE III. Calculated ideal tensile $\sigma$ and shear $\tau$ strengths (in GPa), bulk modulus $B$ (in GPa), and shear modulus $G$ (in GPa) of $Al_4SiC_4$, $Al_4C_3$, and 4H-SiC, together with the strain energy differences $\Delta E = E_t - E_s$ (in eV/formula), where $E_t$ and $E_s$ are strain energies at the maximum tensile and shear stresses, respectively.

| Compound | $B$ | $G$ | $\sigma$ | $\tau$ | $\Delta E$ |
|---|---|---|---|---|---|
| $Al_4SiC_4$ | 179 | 140 | 20 | 18 | −0.415 |
| $Al_4C_3$ | 170 | 129 | 21 | 22 | −1.000 |
| 4H-SiC | 226 | 209 | 48 | 38 | −0.263 |

## IV. IDEAL STRENGTH AND ATOMISTIC DEFORMATION MODES

Material deformation is strain dependent and elastic parameters may not always give accurate account for all macroscopic mechanical properties, such as properties related to atomic plane slip. The reason can be attributed to the fact that these elastic parameters are computed under equilibrium conditions; while material deformation associated with experimental strengths occurs at strains where atomic bonding characteristics change significantly. Therefore, studies of the theoretical stress-strain relationships following a material strained from elasticity to the limit of its structural stability and the underlying atomistic deformation modes are important in understanding structural stability, strengths, hardness, and ductility.

In Fig. 3, we present the calculated Hellmann-Feynman stresses for $Al_4SiC_4$ at various tensile and shear strains, to

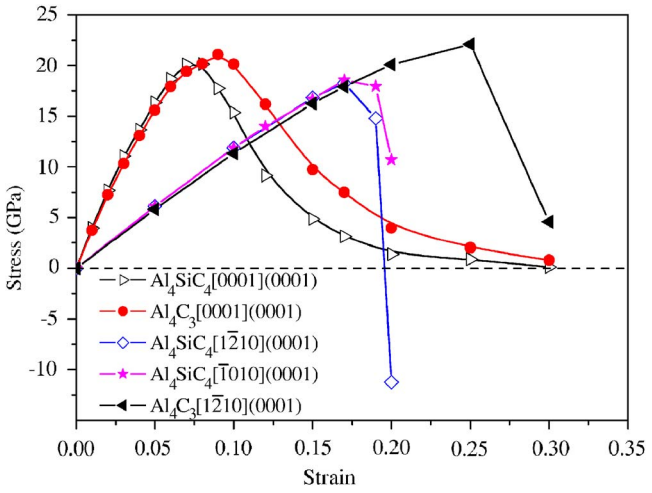


FIG. 3. (Color online) Calculated stress-strain relation for $Al_4SiC_4$ and $Al_4C_3$. Solid circles and empty triangles represent tensile stresses along $c$ direction for $Al_4C_3$ and $Al_4SiC_4$, respectively; empty diamonds and solid pentagons correspond to the shear stresses of $Al_4SiC_4$, for $[1\bar{2}10](0001)$ and $[\bar{1}010](0001)$ slip systems, respectively; and the shear strain in $[1\bar{2}10](0001)$ direction is displayed by solid triangles for $Al_4C_3$.

gether with the data of $Al_4C_3$ for comparison. The tensile strain was imposed along the high-symmetry [0001] direction of hexagonal material. As the lattice constant $c$ increases, the crystal is reconfigured to relax the lateral stresses. The calculated tensile stress-strain curves exhibit similar trends for $Al_4SiC_4$ and $Al_4C_3$, except for larger critical strain sustained by $Al_4C_3$ before stress relaxation. The tensile strength of $Al_4SiC_4$ experienced a slightly lower value of 20 GPa, while, the tensile strength is 21 GPa for $Al_4C_3$, as tabulated in Table III.

For compound with hexagonal symmetry with large $c/a$ axis ratio, basal-plane slip can be activated in the $[1\bar{2}10](0001)$ or $[\bar{1}010](0001)$ direction, depending on which direction is weak and more operative. To distinguish the slip system of $Al_4SiC_4$ with space group $P6_3mc$, we applied shear strain along the $[1\bar{2}10](0001)$ and $[\bar{1}010](0001)$ direction and calculated the theoretical stress-strain relationship as shown in Fig. 3. It is noted that stress-strain curves for $[1\bar{2}10](0001)$ and $[\bar{1}010](0001)$ shear strains are the same up to shear strain of 0.15. Maximum shear stress of $Al_4SiC_4$ achieves at strain of 0.17 simultaneously for the two shear deformation paths. The ideal shear strength for $[1\bar{2}10](0001)$ shear deformation is only 0.3 GPa larger than that of the $[\bar{1}010](0001)$ shear mode. This suggests similar deformation mechanism for the two strain modes. Therefore, we only analyze atomistic deformation modes and electronic structure mechanism for $[1\bar{2}10](0001)$ shear deformation in the present paper for briefness.

A comparison between $Al_4SiC_4$ and $Al_4C_3$ under $[1\bar{2}10]\times(0001)$ shear strain shows resemblance in linear region but a dramatic difference at a large shear strain. Not only the critical strain sustained by $Al_4SiC_4$ differs from that by $Al_4C_3$, but the stress softening beyond the critical strain are also obviously different for the two materials. Along the $[1\bar{2}10](0001)$ shear path for $Al_4SiC_4$, the stress approaches maximum value at a strain around 0.19 and drops abruptly thereafter, suggesting sudden bond-breaking events at large shear strain. The $Al_4C_3$ lattice sustains larger critical shear deformation on the other hand, and the critical shear strain achieves 0.25. The distinguishable stress-strain curve raises a suspicion that shear-induced structural instability should be different for $Al_4SiC_4$ and $Al_4C_3$ under applied $[1\bar{2}10]\times(0001)$ shear strain. Due to the less sustained critical strain, the ideal shear strength of $Al_4SiC_4$ is 4 GPa smaller than that of binary carbide $Al_4C_3$, which are 18 GPa and 22 GPa, respectively.

It is noticeable in Fig. 3 that bond softening occurs earlier under tensile strain, compared to the case of under shear strain. Hence it is of interest to distinguish the two atomistic deformation modes, i.e., tension and shear, because the stress-strain curves yield obviously different tendency. A tension-induced lattice failure would probably result in cleavage, whereas a shear-induced instability may homogeneously nucleate defects, such as dislocation. The failure mode of a material depends on which type of lattice instability being encountered first. The ideal strength, i.e., the stress at which a perfect crystal becomes mechanically unstable, corresponds to the inflexion point along energy surface with respect to the applied strain. The knowledge of strain energy at the maximum stress may provide insights into the mechanism of preferred failure modes. With the calculated strain energy, one can evaluate the competition between the tensile and shear deformation modes, and thus predict either ductile or brittle response of a solid is allowed.[32] In our previous works,[22] we have revealed that for brittle binary ceramic as TiC, the ratio of ideal tensile to shear strength is nearly unitary. By comparing the strain energies, at which the maximum tensile and shear stress are achieved, we obtained that tensile strain energy was well below the shear strain energy by 0.058 eV/formula for TiC crystal, implying cleavage may intrude prior to shear instability. In contrast, the strain energies corresponding to ideal tensile strength have higher values by 0.740 and 0.695 eV/formula, respectively, than the shear energies for $Ti_2AlC$ and $Ti_2AlN$, which are machinable ceramics capable of damage tolerance and intrinsic toughness. These results indicate that the shear-induced failure is more energetically favorable and can be reached first upon loading for these two compounds. Based on the same idea, we performed calculations on $Al_4SiC_4$, $Al_4C_3$, and 4H-SiC in the present work, and the tensile strain energies corresponding to critical tensile stresses are determined to be 0.415, 1.000, and 0.263 eV/formula smaller than the shear strain energies at each critical shear stress, respectively, as tabulated in Table III. Therefore, $Al_4SiC_4$ is most likely to fail in tension and hence, suggested cleavage fracture mechanism and intrinsic brittleness. Suppose a perfect crystal is deformed theoretically, one can assess the competition between the uniaxial tension and shear stresses by resolving the stress onto the slip systems and comparing with the ideal strengths. Although ideal shear strength is slightly lower than the tensile strength, by resolving the tensile stress onto the slip systems, the resulting shear stress may be much lower than the ideal shear strength. Therefore, the material is expected to fail by tension. Moreover, it is interesting to note that the

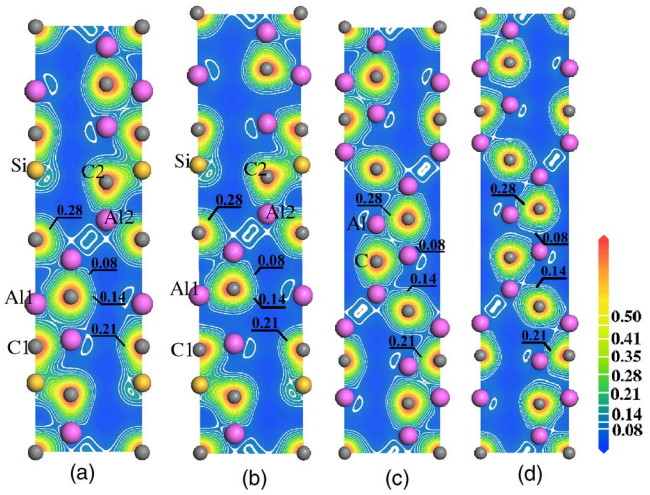


FIG. 4. (Color online) Valence electron density of a slice of the $(11\bar{2}0)$ plane for unstrained $Al_4SiC_4$ is shown in (a); whereas (b) corresponds to the case under applied tensile strain of 0.1 along the $c$ direction. The (c) and (d) figures are similar to (a) and (b) except for $Al_4C_3$. The contour lines range from 0.00 to 0.78 electron/Å$^3$.

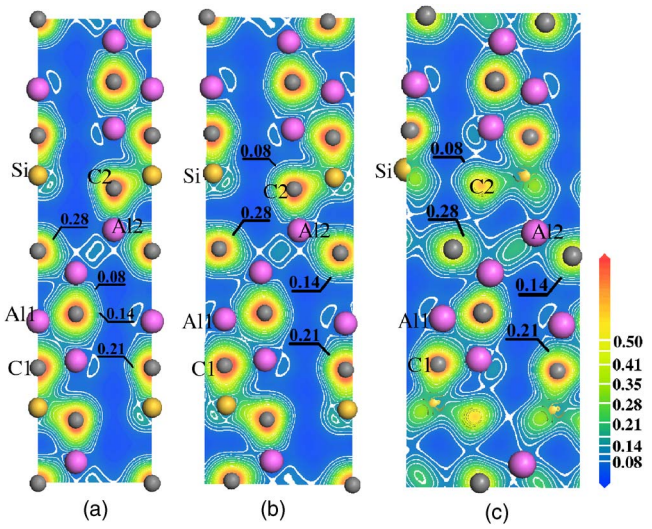


FIG. 5. (Color online) Valence electron density of a slice of the $(11\bar{2}0)$ plane in $Al_4SiC_4$ unit cell under shear deformations of (a) $\varepsilon=0$, (b) $\varepsilon=0.1$, and (c) $\varepsilon=0.2$. The contour lines range from 0.00 to 0.78 electron/Å$^3$.

stress of $Al_4SiC_4$ drops abruptly beyond the critical strain. Such behavior has been frequently experienced by hard or brittle ceramics, such as diamond and *c*-BN.[33]

To further understand the deformation processes at various strains, it is helpful to examine the charge density contours. In Fig. 4, charge density contours of unstrained $Al_4SiC_4$ and $Al_4C_3$ crystals and those under applied tensile strain of 0.1 are illustrated for a slice of $(11\bar{2}0)$ plane. Upon tensile loading, bond-breaking events are indicated by charge depletions from the stretched Al-C bonds, i.e., Al1-C1 bond in $Al_4SiC_4$. This leads to the structural failure of both crystalline at small strains. Because bond breaking occurs inside the $Al_4C_3$-type units in $Al_4SiC_4$, it is likely that $Al_4SiC_4$ and $Al_4C_3$ will show similar mechanical properties that are determined by tension-induced structural instability. In other words, the cleavage of $Al_4SiC_4$ may be originated from the bond-breaking inside the $Al_4C_3$-type unit.

In contrast, the structural failure upon shear strain exhibits different atomistic deformation mechanism for $Al_4SiC_4$, as shown in Fig. 5. The softening and breaking of the Al2-C2 bond, instead of the weakest Al1-C1 bond, lead to the structural instability of $Al_4SiC_4$ under shear deformation. Particularly, the Al2-C2 bond corresponds to the coupling between $Al_4C_3$- and SiC-type structural units. According to previous investigation, we know that the *p* orbital involved covalent bond may behave diversely in response to tension or shear strain.[22] The extensively distributed *p* states of Al-C covalent bond is expected to respond more readily to the shear deformation than to tension. Therefore, a slightly lower shear strength of $Al_4SiC_4$ is obtained compared with tensile strength, despite stronger Al2-C2 bond is involved in shear-induced instability.

## V. CONCLUSIONS

In summary, we investigated the bonding characteristics, elastic stiffness, ideal strengths, and atomistic deformation modes of $Al_4SiC_4$ by first-principles calculations. We show that the mechanical properties are closely related to the crystal structure of $Al_4SiC_4$, which could be described as $Al_4C_3$-type structural units and hexagonal SiC-type units stacked along [0001] direction. The elastic moduli of $Al_4SiC_4$ show more resemblance to its binary counterpart, $Al_4C_3$. Bonding strengths analysis of $Al_4SiC_4$ under various hydrostatic pressures demonstrated a strong coupling between the $Al_4C_3$- and SiC-type structural units. Bond-softening and bond-breaking processes upon tensile and shear deformations were illustrated and compared for $Al_4SiC_4$ and $Al_4C_3$. The results show how interatomic bonds in the ternary carbide respond to applied strains, especially strain near structural instability. Tension-induced bond-breaking occurs inside the constitutive $Al_4C_3$-type structural unit, which provides $Al_4SiC_4$ a similar tensile strength with $Al_4C_3$. On the other hand, shear-induced instability is originated from the coupling bond between $Al_4C_3$- and SiC-type structural units. In addition, the lower strain energy at maximum tensile stress, i.e. ideal strength, than the energies in shear cases, together with deformation modes, suggest cleavage fracture mechanism and an intrinsic brittle character of $Al_4SiC_4$. To better understand the mechanical properties of a material with alternatively stacked structural units, one can trace back to the properties of each constituent structural unit and the coupling strength between them. Both may play a key role in determining the inherent mechanical properties.

## ACKNOWLEDGMENTS

This work was supported by the National Outstanding Young Scientist Foundation for Y. C. Zhou under Grant No. 59925208 and by Natural Sciences Foundation of China under Grant Nos. 50232040, 90403027 and 50302011.

[1] J. F. Huang, X. R. Zeng, H. J. Li, X. B. Xiong, and M. Huang, Mater. Lett. **58**, 2627 (2004).
[2] M. W. Barsoum, Prog. Solid State Chem. **28**, 201 (2000).
[3] J. C. Schuster and H. Nowotny, Z. Metallkd. **71**, 341 (1980).
[4] J. Y. Wang, Y. C. Zhou, Z. J. Lin, T. Liao, and L. F. He, Phys. Rev. B **73**, 134107 (2006).
[5] T. M. Gesing and W. Jeitschko, J. Solid State Chem. **140**, 396 (1998).
[6] S. E. Lofland, J. D. Hettinger, K. Harrell, P. Finkel, S. Gupta, M. W. Barsoum, and G. Hug, Appl. Phys. Lett. **84**, 508 (2004).
[7] Z. M. Sun, D. Music, R. Ahuja, and J. M. Schneider, J. Phys.: Condens. Matter **17**, L15 (2005).
[8] J. Y. Wang and Y. C. Zhou, J. Phys.: Condens. Matter **16**, 2819 (2004).
[9] K. Inoue, S. Mori, and A. Yamaguchi, J. Ceram. Soc. Jpn. **111**, 348 (2003).

[10] K. Inoue, S. Mori, and A. Yamaguchi, J. Ceram. Soc. Jpn. **111**, 126 (2003).
[11] O. Yamamoto, M. Ohtani, and T. Sasamoto, J. Mater. Res. **17**, 774 (2002).
[12] K. Inoue, A. Yamaguchi, and S. Hashimoto, J. Ceram. Soc. Jpn. **110**, 1010 (2002).
[13] V. L. Solozhenko and O. O. Kurakevych, Solid State Commun. **135**, 87 (2005).
[14] S. H. Jhi, J. Ihm, S. G. Louie, and M. L. Cohen, Science **399**, 132 (1999).
[15] D. Roundy, C. R. Krenn, M. L. Cohen, and J. W. Morris, Phys. Rev. Lett. **82**, 2713 (1999).
[16] S. Ogata, J. Li, N. Hirosaki, Y. Shibutani, and S. Yip, Phys. Rev. B **70**, 104104 (2004).
[17] M. Jahnátek, M. Krajcí, and J. Hafner, Phys. Rev. B **71**, 024101 (2005).
[18] D. M. Clatterbuck, D. C. Chrzan, and J. W. Morris, Acta Mater. **51**, 2271 (2003).
[19] J. Frenkel, Z. Phys. **37**, 572 (1926).
[20] J. H. Rose, J. R. Smith, and J. Ferrante, Phys. Rev. B **28**, 1835 (1983).
[21] G. Xu, A. S. Argon, and M. Ortiz, Philos. Mag. A **72**, 415 (1995).
[22] T. Liao, J. Y. Wang, and Y. C. Zhou, Phys. Rev. B **73**, 214109 (2006).
[23] M. D. Segall, P. L. D. Lindan, M. J. Probert, C. J. Pickard, P. J. Hasnip, S. J. Clark, and M. C. Payne, J. Phys.: Condens. Matter **14**, 2717 (2002).
[24] D. Vanderbilt, Phys. Rev. B **41**, 7892 (1990).
[25] J. P. Perdew, J. A. Chevary, S. H. Vosko, K. A. Jackson, M. R. Pederson, D. J. Singh, and C. Fiolhais, Phys. Rev. B **46**, 6671 (1992).
[26] J. D. Pack and H. J. Monkhorst, Phys. Rev. B **16**, 1748 (1977).
[27] B. G. Pfrommer, M. Cŏté, S. G. Louie, and M. L. Cohen, J. Comp. Physiol. **131**, 233 (1997).
[28] V. Milman and M. C. Warren, J. Phys.: Condens. Matter **13**, 241 (2001).
[29] P. Ravindran, L. Fast, P. A. Korzhavyi, B. Johansson, J. Wills, and O. Eriksson, J. Appl. Phys. **84**, 4891 (1998).
[30] Powder Diffraction File, No. 11-629, Joint Committee on Powder Diffraction Standards, Swarthmore, Pennsylvania (1972).
[31] A. Bauer, J. Krausslich, L. Dressler, P. Kuschnerus, J. Wolf, K. Goetz, P. Kackell, J. Furthmuller, and F. Bechstedt, Phys. Rev. B **57**, 2647 (1998).
[32] A. Kelly, *Strong Solids* (Oxford University Press, London, 1966).
[33] Y. Zhang, H. Sun, and C. F. Chen, Phys. Rev. Lett. **94**, 145505 (2005).